American Mineralogist, Volume 91, pages 12–20, 2006

An FTIR study of hydrogen in anorthoclase and associated melt inclusions

SHEILA J. SEAMAN,[1,*] M. DARBY DYAR,[2] NEBOJSA MARINKOVIC,[3] AND NELIA W. DUNBAR[4]

[1]Department of Geosciences, University of Massachusetts, Amherst, Massachusetts 01002, U.S.A.
[2]Department of Earth and Environment, Mount Holyoke College, South Hadley, Massachusetts 01075, U.S.A.
[3]National Synchrotron Light Source, Brookhaven National Laboratory, Upton, New York 11973, U.S.A.
[4]Department of Earth and Environmental Science, New Mexico Institute of Mining and Technology, Socorro, New Mexico 87801, U.S.A.

ABSTRACT

High-resolution Fourier transform infrared (FTIR) spectroscopy has been used to document the presence of hydrogen, to estimate its concentration, and to document its oxygen speciation in anorthoclase crystals and associated melt inclusions from Mount Erebus, Antarctica. Synchrotron-generated infrared radiation, 100 to 1000 times brighter than globar-generated infrared radiation, permits rapid collection of maps that depict relative intensities of a chosen FTIR band across the mapped area. Spectra and/or compositional maps showing variations in water concentration were collected from anorthoclase megacrysts and melt inclusions in the megacrysts. Studies of anorthoclase megacrysts involved collection of spectra from three mutually perpendicular sections cut from the crystals. FTIR spectra of anorthoclase crystals are characterized by a broad absorption band at approximately 3200 cm^{-1} in the mid-IR range. The universal mass absorption coefficient for mid-IR range feldspar spectra, established by Johnson and Rossman (2003), was used for quantitative estimates of water concentrations in the feldspar crystals based on integrated area under the 3200 cm^{-1} band. Water concentration in the anorthoclase sample was approximately 126 ppm, with an overall error of approximately ±30%. FTIR spectra of melt inclusions are characterized by a broad asymmetric absorption band at ~3550 cm^{-1} that was used to calculate total water concentration. The absence of a band at 1630 cm^{-1} suggests that water in the melt inclusions occurs as OH^- rather than as molecular H_2O. Absorption coefficients established by Mandeville et al. (2002) for H species in glass were used to calculate water concentrations in the melt inclusions. Melt inclusions in the Mt. Erebus anorthoclase have water concentrations ranging from 0.12 to 0.39 wt%, with an overall error of approximately ±15%. The ratio of water in anorthoclase crystals to water in the melt from which the crystals formed, based on this study, and at these low melt water concentrations, is approximately 1:10. However, water concentration varies significantly from one melt inclusion to another, possibly suggesting initial melt water heterogeneity. Maps of water concentration show that variations in water concentration within melt inclusions are associated with fractures that cut the melt inclusions and in some cases do not extend out into surrounding crystals or into crystal inclusions. Thin (~50 μm thick) zones of elevated water concentrations on the boundaries of the crystals in contact with melt inclusions suggest that water has diffused into the crystals from the melt inclusions.

Keywords: Water, FTIR spectroscopy, anorthoclase, Mt. Erebus

INTRODUCTION

The water concentration of melts is the major controlling influence on their crystallization temperature, sequence of crystallizing minerals, viscosity, and explosivity. Knowledge of water concentration is central to most studies of magmatic systems, but it is a difficult parameter to constrain. The most common means of making estimates of water concentrations in melts have been: (1) using the mineral assemblage to estimate water concentration on the basis of experimental modeling of igneous systems (e.g., Naney et al. 1983; Whitney 1988; Scaillet et al. 1995; Gardner et al. 1995; Cottrell et al. 1999), (2) measuring water concentrations in melt inclusions (e.g., Anderson 1989; Dunbar and Hervig 1992; Borisova et al. 2002; Fedele et al. 2003; Walker et al. 2003), and (3) measuring gas concentrations at volcanic vents (e.g., Goff et al. 1998; Burton et al. 2000). Experimental work using natural samples provides constraints on pre-eruptive water concentration but depends critically upon knowledge of the temperature, pressure, and oxygen fugacity of the system. Measurements of water concentrations in melt inclusions are possible only in relatively young igneous rocks in which the glass has not yet devitrified, and in melt inclusions that have not leaked water since quenching. Measurement of gas species and concentrations is difficult and can be done only on active igneous systems. The ideal means of knowing water concentration in a melt would be to measure its concentration directly in some mineral phase that faithfully records variations in water concentrations throughout the crystallization sequence. Feldspar may be the appropriate mineral because it is the most common mineral in the Earth's crust, it occurs in felsic to mafic rocks, and it typically spans almost the entire range of crystallization from highest to lowest temperature. Feldspars, particularly plagioclase feldspars, have been used innovatively to document magmatic

* E-mail: sjs@geo.umass.edu

0003-004X/06/0001–12$05.00/DOI: 10.2138/am.2006.1765

processes on the basis of Ca/Na variation (Wiebe 1968; Anderson 1983; Singer and Pearce 1993; Brophy et al. 1996). The present study is a first step in attempting to use feldspars to document variations in parent melt water concentration.

In most felsic magmatic systems, feldspar is the first "anhydrous" mineral to crystallize. Based upon the work of Hofmeister and Rossman (1985) and Kronenberg et al. (1996), we know that feldspar, while nominally anhydrous, can contain H at the ppm level. As observed by Bell and Rossman (1992), structural water has a major effect on the strength of crystalline materials and on their diffusion coefficients. Hence, a significant amount of structural water in feldspar crystals may play a controlling role on strength and other properties of the Earth's crust.

The goal of this work is to use FTIR analyses of anorthoclase crystals and of the glass inclusions they host to examine the equilibrium of water in feldspar crystals and in coexisting melt inclusions, as well as to present observations concerning the behavior of water during quenching and crystallization of feldspar-producing phonolitic magma. We also explore the extent to which water concentration in a melt is homogeneous, and the extent to which it reflects the effects of the local compositional and physical environment. Our analyses of hydrogen are based both on quantitative analysis and on mapping of variations in water concentrations. The maps show particularly striking variations in water concentrations between, and in some cases, within these materials, and provide a means of testing hypotheses about the behavior of water during magmatic processes.

The importance of water in nominally anhydrous minerals

The presence of water in "nominally anhydrous" minerals (those for which water is not part of the structural formula) has been documented spectroscopically in a series of studies over the past several decades (Kats 1962; Dodd and Fraser 1967; Wilkins and Sabine 1973; Chakraborty and Lehmann 1976; Aines and Rossman 1984; Mackwell and Paterson 1985; Smyth 1987; McMillan et al. 1991; Smyth et al. 1991; Nakashima et al. 1995; Ihinger and Zink 2000). Bell and Rossman (1992) documented the presence of small concentrations of OH as structural components of several mantle minerals, including garnet, olivine, enstatite, and omphacite. They evaluated the effect of small amounts of structural water on partial melting of mantle rocks and on Earth's degassing history, and argued that hydrous mantle minerals are effective vehicles for transporting subduction zone water to the lower mantle.

The feldspars are the most abundant group of minerals in the Earth's crust. Feldspars crystallize over most of the range of crystallization temperatures of most magmas. Their crystallization drives the compositional evolution of magmas and is the main reason that the Earth has buoyant continental crust. Water in feldspar is likely to be as important in terms of influencing mechanical strength, melting conditions, diffusion rates, and electrical properties in the crust as hydrous mantle minerals are in the mantle.

Methods

Identification of water in anorthoclase crystals and in melt inclusions was done by FTIR spectroscopy. Spectra were collected at the National Synchrotron Light Source at Brookhaven National Laboratory using infrared radiation generated by the UV-IR synchrotron. The spectrometer endstation is a Nicolet Magna 860 Step-Scan FTIR and Spectra Tech Continuum IR microscope. The synchrotron-generated beam is 100 to 1000 times brighter than that generated by a globar (black body) source in a conventional FTIR. The extra brightness permits better spatial resolution (3–10 μm), better spectral resolution (to 1 cm^{-1}), smaller analytical spot size (to 8 μm^2), and faster spectrum collection (~1 min.) compared to a conventional IR source. In this study, spectra were collected in the mid- and near-IR ranges (1500–6000 cm^{-1}) using a KBr beamsplitter and an internal DTGS-KBr detector. Quantitative evaluation was done only on bands in the mid-IR range (1600–4000 cm^{-1}) because the sensitivity of the available detector is greatly reduced in the near-IR range.

The sum of absorbances measured in three orthogonal sections through a crystal is necessary for quantitative analysis of water concentration (Libowitzsky and Rossman 1997). Polarized radiation provides the best quantitative data for analysis of crystals (Dowty 1978). Synchrotron-generated IR radiation is approximately 80% polarized (L. Miller, pers. comm., 2003). The orientation of the plane in which the IR radiation predominantly vibrates is vertical and east-west; the sample lies in a horizontal plane. Johnson and Rossman (2003) showed experimentally that, although polarized measurements with the electric vector vibrating parallel to the three principal optical directions are preferred, any three mutually perpendicular spectra will give the same integrated band area within ±5% relative error. In this study, we measured spectra in three mutually perpendicular sections that were chosen to correspond as nearly as possible to the crystallographic axes of anorthoclase, with synchrotron-generated radiation that is not entirely polarized. Hence, water concentrations calculated on the basis of the sum of the integrated band areas of each of the three orientations are likely to provide slight overestimates of water concentrations. Quantification of the amount of overestimation is difficult, but the amount of the overestimate should be considerably less than 30% because OH pairs are not isotropic in shape, and hence will not intercept the maximum possible incident IR radiation in each of the three crystal orientations.

The samples that were analyzed are self-supported thin slices of rock, of conventional thin section dimensions, and ranging in thickness from 0.013 to 0.023 cm. Samples were prepared using the same procedure typically used for preparing a thin section, except that acetone-soluble epoxy (Crystalbond, product number 509) was used for cementing the rock to the glass slide. After polishing to the appropriate thickness, each slide was placed in an acetone bath until the rock slice separated from the glass. Each slice was carefully extracted from its acetone bath and was allowed to dry thoroughly before analysis. Exact (±1 μm) thickness of the samples was determined by measurement with a Starrett no. 733 digital micrometer. The slices were supported by being placed between two glass slides into which central holes had been drilled. FTIR spectra were first examined to ensure that they do not include bands indicative of C-H groups, which would indicate the presence of undissolved epoxy that might itself contain exotic water. Spectra were collected from discrete points on the crystals and melt inclusions. In addition, maps showing variations in the integrated areas under the broad absorption peak (~3000–3700 cm^{-1}) from which total water was calculated were interpreted to show areal variations in total water concentration.

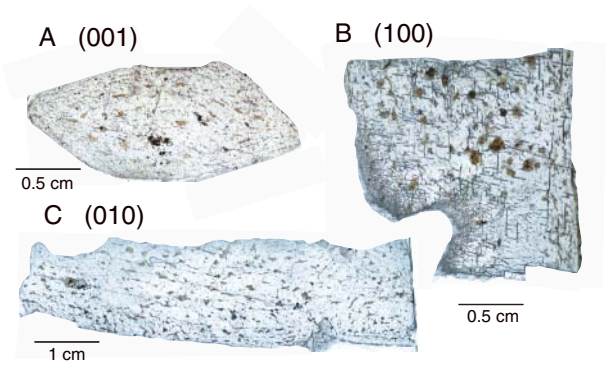

Figure 1. (**a**, **b**, **c**) Photographs of three mutually perpendicular sections of Mount Erebus anorthoclase. The amber spots are melt inclusions, some of which host mineral inclusions. Some melt inclusions are cut by fractures that represent the cleavage of the anorthoclase crystal. Other melt inclusions have internal fractures that seem not to extend out into the surrounding crystal.

During both map collection and single point analyses, aperture sizes ranged from 10 × 10 to 15 × 15 μm and step size was always chosen to be smaller than the aperture width, typically 8 to 13 μm. The infrared beam was focused onto the aperture, and was then refocused onto the sample with the infrared objectives. As a result, the infrared light converged to minimum size in the plane of focus and then diverged again as it passed downward through the sample. Thus the excitation volume has the geometry of a convergent and divergent cone. If the numerical aperture (N.A.) of the objective is 0.65, and the refractive index of the sample (n) is 1.5, then the angle at which the beam converges to minimum size θ, is approximately 26° (N.A. = n sin θ). Thus, if the beam were focused on the median plane of a 70 μm thick sample, the beam size at the upper and lower surfaces would be approximately 34 × 34 μm. If the beam were focused on the upper surface of the sample, the area sampled on the bottom of a 70 μm thick sample would be approximately 68 × 68 μm. Objects analyzed in and near the plane onto which the aperture is focused are analyzed with greatest resolution, but less intense IR radiation affects material in the divergent cone, and information generated in that cone is part of the resultant spectrum. As a result, the map resolution is close to the focused beam size with a lower-resolution continuum coming from the deeper parts of the sample. The Nicolet Continuum microscope, used in this study, has apertures both before and after the sample to eliminate diffraction effects that are introduced by the aperture. In analyzing the large homogeneous regions of anorthoclase crystals and melt inclusions in this study, the conical increase in sampling volume across the thickness of the sample poses little problem. However, its effects on overall analytical resolution have to be considered in studies of smaller and/or less homogeneous objects.

Two large (~9 cm long), melt inclusion-bearing anorthoclase crystals from Mount Erebus were analyzed. The crystals were cut in three mutually perpendicular orientations, as close as possible to (100), (010), and (001), and spectra were collected from both the crystal and from melt inclusions in each of the orientations. Hydrogen concentration calculations were based on the sum of H concentrations deduced from each of the three mutually perpendicular orientations, as suggested by Libowitzsky and Rossman (1997) and Johnson and Rossman (2003). In the second part of the study, spectra and compositional maps were collected from melt inclusion glass.

The concentration of O-H species from which water concentration can be calculated can be related to the height of or the area under peaks representing H-O bending or stretching on an FTIR spectrum (intensity vs. frequency) by the Beer-Lambert Law:

$$A = c * t * \varepsilon \quad (1)$$

where A is the absorbance measured from spectra from each of the three mutually perpendicular sections, c is the concentration of the species, t is the thickness, and ε is the molar absorption coefficient. Following the approach used by other workers, in this study we used the integrated area under the peak to calculate water concentrations in the crystals (Libowitzsky and Rossman 1997; Johnson and Rossman 2003) and the height of the peak to calculate water concentration in glass (Stolper 1982; Dixon et al. 1988; Ohlhorst et al. 2001; Mandeville et al. 2002). The following form of the Beer-Lambert Law was used to calculate water concentrations in crystals (Libowitzsky and Rossman 1997):

$$c\ (\text{wt\% } H_2O) = A\ (\text{cm}^{-1}) \cdot 1.8 / [t(\text{cm}) \cdot D(\text{g/cm}^3) \cdot \varepsilon\ (\text{cm}^{-2}/\text{mol } H_2O\ \text{L}^{-1})] \quad (2)$$

where D is density and A is the area under the absorption peak. The following form of the Beer-Lambert Law was used for calculating water concentration in glass (Stolper 1982):

$$c\ (\text{weight fraction}) = \{(18.02 \cdot \text{Absorbance}) / [d\ (\text{cm}) \cdot \rho\ (\text{g/liter})]\} \cdot [1/\varepsilon\ (\text{liters/mol-cm})] \quad (3)$$

where absorbance is the height of the absorption peak. For isotropic materials such as glasses (quenched melts), any optical direction should have the same value for A, and hence OH^- and H_2O complexes should have no crystallographic preferred orientation. Thus, the water concentration of a glass can theoretically be measured with a single FTIR spectrum while that of a crystal is related to the sum of the area under the peaks for each of three mutually perpendicular orientations. Johnson and Rossman (2003) established a universal absorption coefficient for feldspars (107 000 ± 5000 L/molH_2O-cm^{-2}) that can be used in the Beer-Lambert law for calculation of water concentration using the sum of maximum band heights around 3200 cm^{-1} measured parallel to the three principal optic axes. Their measurements of band heights of unpolarized IR spectra yielded a linear relationship (slope = 6.7) between band area and ppm of H_2O on the basis of measurements of sanidine and microcline. Measurements of albite are in agreement with the linear trend, but measurements of other compositions of plagioclase fall off of the trend (Johnson and Rossman 2003). Johnson and Rossman (2003) concluded that band areas measured with unpolarized radiation provide a rough estimate of hydrogen concentrations for alkali feldspar but that, with the exception of albite, the method does not work well for members of the plagioclase series.

Several workers (Stolper 1982; Newman et al. 1986; Zhang et al. 1997; Ohlhorst et al. 2001; Mandeville et al. 2002) have established molar absorption coefficients for both near-IR (5200 cm^{-1} and 4500 cm^{-1}) bands and mid-IR (3200–3500 cm^{-1}) bands in glasses. In this study, the molar absorption coefficients of Mandeville et al. (2002) was used for the 3200–3500 cm^{-1} band because the composition of the phonolitic Mt. Erebus glass closely matched a range of the andesitic glasses that were the subject of their study. Bell and others (1995) evaluated the sources of uncertainty in quantitative analysis of OH in garnet and pyroxene. Their analysis is valid as well for analyses of feldspars and similarly anhydrous minerals with variability in spectra associated with compositional and structural variety. The error in determining total integrated area has been estimated to be less than 10%, and the possible error in the absorption coefficient (Johnson and Rossman 2003) is approximately 5% (10 7000 ± 5000). Standard error propagation through Equation 2 then suggests that:

$$\Delta c/c = \Delta A/A + \Delta\varepsilon/\varepsilon \quad (4)$$

where Δc is the maximum error in the obtained result. We suggest that a liberal estimate of the additional error incurred (in measurements of H in crystals only) by using unpolarized radiation would be ±15%. Considering all error sources, the maximum error for calculation of water in anorthoclase crystals is approximately ±30%, assuming that errors are uncorrelated. Precision of analyses of total water in glass is approximately ±5%. Dixon and others (Dixon et al. 1991; Dixon and Clague 2001) estimated the accuracy of total water analyses as ±10% based on the accuracy of absorption coefficients. Propagation of error estimates in determining the band areas (±10%) and in the molar absorption coefficients (±10%) through Equation 3 yields total accuracy estimates of ± 20% for total water in glass.

RESULTS

Anorthoclase from Mt. Erebus

Geologic context. FTIR spectra were collected from three slices parallel to the three principal crystallographic axes through an anorthoclase megacryst from Mt. Erebus, Antarctica (Figs. 1a-c). Anorthoclase megacrysts from Mount Erebus are 4–8 cm long and are phenocrysts in phonolitic vessels erupted from the vent in 1984 (Dunbar et al. 1994). The megacrysts contain abundant large (to 5 mm) amber colored melt inclusions. Dunbar et al. (1994) analyzed anorthoclase crystals and melt inclusions and measured water concentrations in melt inclusions using an ion microprobe. They found water concentrations in melt inclusions ranging from 0.1 to 0.3 ± 0.1 wt% (1000–3000 ppm ± 1000 ppm) and concluded that the anorthoclase megacrysts grew relatively rapidly, but in two stages. They found no variation in melt inclusion composition depending on position in the host crystals, and found that the melt inclusion composition is identical to that of matrix glass. Based on the low volatile concentrations of the melt inclusions, they concluded that the crystals grew at low (<300 bars) pressures.

Hydrogen speciation in Mt. Erebus anorthoclase crystals. The most prominent absorption band produced by anorthoclase crystals in this study is the broad symmetric peak centered at approximately 3250 cm^{-1} (parallel to Z > parallel to X, Y) (Fig. 2). The ~3500 cm^{-1} peak results from either X-OH groups or H-O-H groups (Stolper 1982). On the basis of the constancy of the

relationship between the height of this peak and total water concentration, Stolper (1982) suggested that the height of the peak could be used to determine total water concentrations of silicate glasses. Other workers (e.g., Dixon et al. 1988; Mandeville et al. 2002) have used the peak in this way, and it has been used to calculate total water concentrations in anorthoclase crystals and in melt inclusions (described below) in this study.

The concentration of water calculated using the Beer-Lambert Law and the molar absorption coefficient of Johnson and Rossman (2003), based on the area under the 3200 cm^{-1} peak, covers approximately the same range (27–60 ppm) for each of the three crystallographic orientations for which spectra were collected (Table 1). Using an average value of water concentrations for each of the three orientations, and summing these values, we arrived at a water concentration of 126 ppm ± 38 ppm for Mt. Erebus anorthoclase crystals.

Hydrogen speciation in Mt. Erebus melt inclusions. The most prominent peak in FTIR spectra of melt inclusions is a broad asymmetric peak centered at approximately 3300 cm^{-1}, but with its inflection point at approximately 3550 cm^{-1} (Fig. 3). This peak was used to calculate total water concentrations in melt inclusions. Molar absorption coefficients have been established for the 3550 cm^{-1} band as well as for a molecular water band at 1630 cm^{-1} by several workers (Stolper 1982; Newman et al. 1986; Zhang et al. 1997; Ohlhorst et al. 2001; Mandeville et al. 2002). The molar absorption coefficients of Mandeville et al. (2002), 62.32 ± 0.42 L/mol-cm for the 3500 cm^{-1} peak and 42.34 ± 2.77 for the 1630 cm^{-1} peak, were used in this study.

The water concentrations in melt inclusions in Mt. Erebus anorthoclase crystals is 0.12 to 0.39 wt% on the basis of application of the Beer-Lambert law to the height of the 3500 cm^{-1} peak and use of the molar absorption coefficient of Mandeville et al. (2002). This range of values agrees closely with water concentrations measured in these melt inclusions by Dunbar et al. (1994) using the ion microprobe. The 1630 cm^{-1} peak, also a product of molecular water, is absent in spectra collected from melt inclusions in this study (Fig. 3), suggesting that molecular water is not present in these inclusions, and that essentially all of the water is in the form of OH molecules. This is consistent with the relationship between higher overall water concentrations and higher molecular water concentrations (and vice-versa) in melts and crystals (Stolper 1982).

Interpretation of compositional maps. Maps of water concentrations in melt inclusions (Fig. 4) show that water concentration can be heterogeneous within melt inclusions. The main cause of heterogeneity in water concentration in the melt inclusions observed in this study is the presence of fractures, many of which cut only the melt inclusions and do not extend

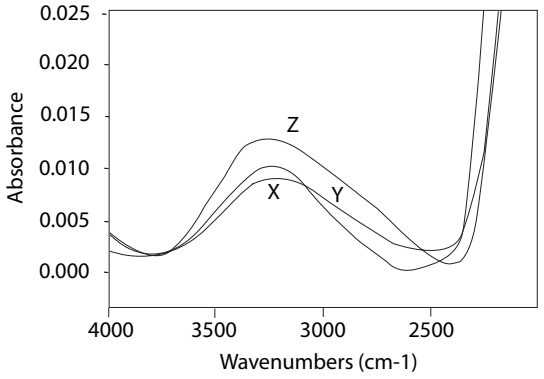

FIGURE 2. Mid-IR spectra of anorthoclase from Mount Erebus, with the polarization direction of the IR radiation oriented parallel to the X, Y, and Z vibration directions of light passing through the anorthoclase crystal.

TABLE 1. FTIR spectroscopic data and calculated water concentrations

Erebus Anorthoclase (density ~ = 2.58 g/cm^3; absorption coefficient = 107000 ± 5000 L/mol H_2O cm^2)			**Erebus Melt Inclusions** (density ~ = 2.37 g/cm3; absorption coefficient = 62.32 L/mol H2O cm)		
a parallel to IR vibration direction; thickness = 0.023 cm; band: 3450/cm					
point number	IR band area (/cm)	ppm water	point number	IR band height	ppm water
w13p1	7.36	34	w6p1	0.183	1480
w13p2	13.02	60	w6p2	0.447	3630
w13p4	7.97	37	w6p3	0.143	1160
w13p5	9.57	44	w6p4	0.255	2070
w13p6	9.48	44	w6p5	0.218	1770
	Average	44	w10p6	0.153	1240
	St. Dev.	10	w10p7	0.168	1360
			w10p8	0.157	1270
b parallel to IR vibration direction; thickness = 0.014 cm; band: 3450/cm			w10p9	0.145	1120
point number	IR band area (/cm)	ppm water	w12p6	0.079	640
w10p2	*12.81*	58	w12p7	0.29	2350
w10p3	8.74	40	w12p8	0.156	1270
w10p4	7.25	33	w12p9	0.051	410
w10p5	9.77	45	w12p10	0.111	900
	Average	44		Average	1476
	St. Dev.	11		St. Dev.	803
c parallel to IR vibration direction; thickness = 0.013 cm; band: 3450/cm					
w11p1	12.43	57			
w11p2	9.54	44			
w11p3	7.17	33			
w12p1	10.17	27			
w12p2	14.28	38			
	Average	40			
	St. Dev.	11			

Note: Water concentration of Erebus anorthoclase based on total integrated area under bands: ~128 ppm.

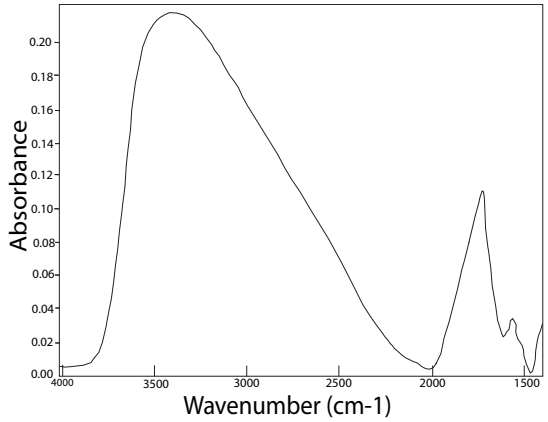

FIGURE 3. Mid-IR spectrum of a melt inclusion from a Mount Erebus anorthoclase. The large peak centered at approximately 3500 cm^{-1} was used to calculate total water concentration. Water is interpreted to exist essentially entirely as OH complexes in the melt inclusions because there is no molecular water peak at 1630 cm^{-1}.

out into the surrounding crystal, and others that represent the intersection of cleavage with melt inclusions. The melt inclusions themselves migrated along cleavage planes in the crystal [compare the (100) section in Figure 1 with either the (010) or (001) sections]. However, it does not appear that water leaked significantly from the melt inclusions into the crystal along cleavage planes. Rather, the largest gradations in water concentrations appear within melt inclusions, and near fractures that cut that inclusion. For example, the gradation in water concentrations represented in Figure 4a from the highest concentration zones in fractures (shown in blue) to the lowest concentration (shown in pink), adjacent to crystals, is from approximately 3900 to 200 ppm. Despite this variety, there are large plateaus of nearly constant water concentration in melt inclusions that are not cut by fractures, and these features provide the opportunity to measure overall water concentration in each inclusion.

There is significant variation in water concentrations from one melt inclusion to another. The possibility exists that this inter-inclusion variation in melt water concentration represents trapping of inclusions at different times during the crystallization history, with crystals migrating through convecting magma and sampling melt of varying water concentrations at different times. Water concentrations were measured in ten melt inclusions that form a traverse from the center to the edge of a (100) anorthoclase section. The water concentrations in the central melt inclusions (shown in Fig. 4a) ranges from 3900 to 400 ppm, but outside of fracture zones, in "plateau" areas of little concentration varia-

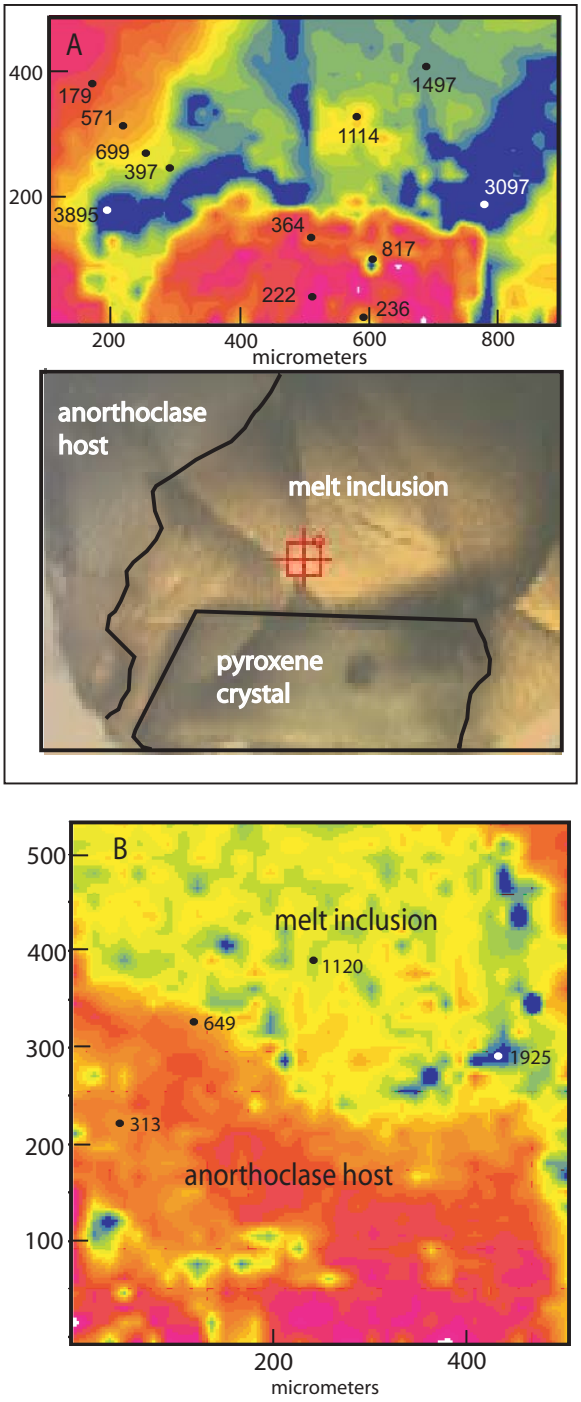

FIGURE 4. (**a**) Compositional map (top) and optical image (bottom) of part of a melt inclusion, host anorthoclase, and a pyroxene crystal included in the melt inclusion from a (100) section through an anorthoclase crystal. Blue represents the highest concentration of total water; pink represents the lowest concentration of total water. The wide gradational zone of water concentrations between melt inclusion and anorthoclase in the upper left of the compositional map is most likely an artifact of beveling of the crystal/melt inclusion boundary and/or divergence of the beam below the surface of the sample. Fractures in the melt inclusion are sites of high water concentration. Concentrations of water are shown in parts per million. Note the small melt inclusion in the pyroxene crystal. (**b**) Compositional map of part of a melt inclusion and part of the host anorthoclase crystal from a (010) section through an anorthoclase crystal. There is an approximately 50 µm wide zone of gradational water concentrations on the edge of the anorthoclase crystal, most likely due to diffusion of water into the crystal from the melt inclusion and/or to divergence of the beam below the surface of the sample. Water concentrations are shown in parts per million.

tion in the melt inclusion, the concentration is approximately 1500 ppm. Melt inclusions encountered on the traverse from this central inclusion to the edge have concentrations that seem to randomly vary from 1220 ppm to 930 ppm to 1500 ppm down to 360 ppm and back up to 910 ppm as the edge is approached. These variations may mirror some subtle zoning in the crystal that itself occurred in response to changes in the magma water concentrations, but we found evidence of no such zoning in the crystal immediately adjacent to each inclusion. Nonetheless, a more extensive study of controls on variation of melt inclusion water concentrations from inclusion to inclusion is warranted. If it is truly spatially random, the variation in water concentrations from one melt inclusion to another may imply heterogeneity in water concentrations in silicic melts in general.

Because it is influenced by surrounding and included minerals and fractures that typically do not extend out into the surrounding mineral, the intra-inclusion water concentration heterogeneity almost certainly developed after the melt was trapped in the host mineral. In one example (Fig. 4a), a pyroxene crystal is present inside of a melt inclusion, itself trapping a small melt inclusion that stands out as being water-rich. A survey of water concentrations in melt inclusions in the (100) section of the Mt. Erebus anorthoclase indicated that "average" water concentrations (measured in plateau zones in the interior of inclusions, away from crystal boundaries) vary widely from one melt inclusion to another (from approximately 358 to 3000 ppm, a similar range to that documented across the water concentration gradation in Fig. 4a), and that there appears to be little spatial control with respect to position of the melt inclusion in the host crystal on concentration. In this small sampling, no water-poor inclusions (<1000 ppm) were found in the cores of anorthoclase crystals, but high water-rich inclusions (>1000 ppm) were found throughout the crystals.

Water is concentrated along fractures. In some instances these fractures appear to be entirely contained in the melt inclusion and do not extend out into the surrounding anorthoclase crystal. These fractures may be a result of contraction upon cooling and quenching of the melt. Because the fractures are restricted to inclusions, water apparently migrated to these fractures after the fractures formed. There is no indication that water was exsolved from the melt at the time when it migrated to the fracture zones. The large anorthoclase phenocrysts certainly grew before the host magma erupted. However, Dunbar and others (1994) used the low water concentrations of the melt inclusions to argue that the magma was stored at a shallow depth, where it had largely degassed by the time the anorthoclase crystals grew. The anorthoclase crystals themselves would have served as pressure vessels for the little water left in the magma at the time of their crystallization. Based on the solubility of water in phonolitic melt, Dunbar et al. (1994) calculated that the crystals grew from largely degassed magma at no greater than 400 m depth. As the melt and its anorthoclase crystals rose to shallower depths and eruption occurred, the confining pressure of the anorthoclase crystals on the melt inclusions is likely to have kept the water dissolved in the melt. If this was the case, migration of water to the fractures in the melt inclusions presumably took place by OH molecules diffusing through the glass.

In general there is little variation in water concentrations along the boundaries between melt inclusions and crystals, regardless of whether the mineral is inside of the melt inclusion or in the host mineral that surrounds the inclusion (Fig. 4b). The wide (~170 μm) progressively decreasing water concentration zone between the melt inclusion and host anorthoclase (upper left of Fig. 4a) is most likely an artifact of beveling of the crystal/melt inclusion boundary coupled with sampling of larger areas with greater depth in the sample as a result of the conical shape of the beam as it passes through the sample (discussed above).

Considering the range in overall water concentration from one melt inclusion to another, and the heterogeneity in melt inclusion water concentration that it suggests, it may be surprising that more of a range of water concentrations is not preserved within most melt inclusions. Apparently diffusion of H_2O and OH over the past ~3000 years, since crystallization of the anorthoclase and quenching of the melt inclusions, has largely eliminated any heterogeneity in H_2O and/or OH concentrations that may have existed within the melt inclusions. Gradations in water concentrations seem to be preserved in zones adjacent to high water-concentration fractures and within minerals that border melt inclusions (Fig. 4a)

Calculations regarding diffusion rates for H_2O and OH indicate that although molecular water diffuses much more rapidly than OH, diffusion of either species through rhyolitic glass is rapid enough that total water concentrations should be homogeneous across melt inclusions. Diffusion coefficients for molecular water in rhyolitic glass from Mono Craters have been measured at $\log D_i$ (m^2/sec) = –14.59 ± 1.59 (Zhang et al. 1991) over a temperature range of 400–850 °C, and in rhyolitic glass from New Mexico at –10.90 ± 0.56 (Jambon et al. 1992), over a temperature range of 510–980 °C. Using these coefficients (in the absence of data for diffusion of water through phonolitic glass) and an elapsed time of 3000 years since the host anorthoclase crystallized, we can estimate the extent of diffusion on the basis of a simplification of Fick's second law (Brady 1995):

$$x = (D_i\, t)^{0.5} \quad (5)$$

Using a value of $D_i = 3.16 \times 10^{-13}$ m^2/s (Jambon et al. 1992) this approximation suggests that compositional equilibration would occur throughout a sphere of radius 1 mm in only 37 days. A very short time period (2.6 minutes) would be required to produce equilibration using a value of $D_i = 6.31 \times 10^{-9}$ m^2/s (Zhang et al. 1991). These diffusion coefficients apply to diffusion of water at a temperature of 1200 °C. It is reasonable to expect that these crystals remained at approximately this temperature, near the liquidus of feldspar in phonolite, over much of their 3000 year lifetime prior to eruption. Lack of data about diffusion coefficients of water in phonolitic glass clearly introduces uncertainty into these estimates, but the less polymerized nature of phonolitic melt compared to rhyolitic melt suggests that diffusion in phonolitic glass would be faster than in rhyolitic glass.

Zhang and others (1991) explored the role of speciation in water diffusion in rhyolitic glass and melt at relatively low total water concentrations (0.1 to 1.8%), surface pressure (0.1 MPa), and 400–550 °C. They derived the following expression to describe the diffusion of H_2O:

$$\partial X/\partial t = \partial/\partial x \left[D_{H_2Om} \partial X_m/\partial x + D_{OH} (\partial X_{OH}/2)/\partial x \right] \quad (6)$$

where D_{H_2Om} is the diffusivity of molecular H_2O, D_{OH} is the diffusivity of OH complexes, and X, X_m, and X_{OH} are mole fractions of total water, molecular water, and OH. Zhang et al. (1991) determined that the diffusion coefficient of OH groups is negligible, on the basis of dehydration experiments. Hence:

$$D_{H_2Ot} = D_{H_2Om} \partial X_m/\partial X \quad (7)$$

where D_{H_2Ot} is total H_2O diffusivity. Studies of water diffusion in melts have generally considered molecular water, rather than OH, to be the diffusing species in systems ranging from rhyolitic (Zhang et al. 1991; Zhang and Behrens 2000) to basaltic (Zhang and Stolper 1991), despite the fact that OH is the much more abundant species at low water concentrations. We suggest that the appearance of gradations in water concentrations in fractured melt inclusions is a combined effect of (1) viewing and mapping fracture zones that are not perpendicular to the surface of the sample through a moderately thick section of glass and (2) the presence of microfractures and possibly zones of greater and lesser strain within the melt inclusions. The fractures show greatest water concentration where the fracture surfaces intersect the surface of the sample, and gradationally lower concentration as the fracture surface curves to the interior of the sample. In addition, it seems likely that discontinuities in the glass (including fractures that are too subtle to be visible microscopically) are sites of greater water concentration; these features may be spatially associated but not coincident with the optically visible fractures.

Diffusion of water was not limited to the melt inclusions; zoning in water concentration in the host anorthoclase and in the anhydrous minerals in the melt inclusions, shown in the compositional maps, may be the result of slow diffusion of water into these anhydrous minerals. The edges of both host anorthoclase and pyroxene inclusions (Figs. 4a and 4b) typically show a zone of decreasing water concentration toward the crystal that is about 50 μm in width. Derdau and others (1998) established rates of oxygen diffusion in "dry" sanidine feldspar (as opposed to "wet" sanidine in a hydrothermal setting) and discussed oxygen diffusion rates in comparison to rates of OH diffusion in sanidine feldspar. They found that oxygen diffuses through interstices in the crystal structure of the feldspar and that oxygen diffusion in sanidine follows an Arrhenius relationship of the form $D = 8.4 \times 10^{-11} \exp(-245 \pm 15 \text{ kJ/mol}/RT) \text{m}^2\text{s}^{-1}$. They found the diffusion rate of oxygen to be slower in anorthite than in sanidine, which probably indicates that the diffusion rate in anorthoclase would also be slower than in sanidine. Using their Arhennius expression, water concentration could be expected to equilibrate through a 1 mm diameter volume in 17.4 million years. The migration energies (E in the Arrhennius expression) for OH transport in albite are approximately half the value of those for the oxygen ion, indicating that the diffusion rate of OH in albite (comparable to sanidine) would be about twice as fast as that of O (Derdau et al. 1998). Using the diffusion coefficient of Derdau et al. (1998) to calculate the amount of time required to diffuse oxygen across a 50 μm distance (comparable to the border zone of water gradation on the crystal/glass boundaries in our study) results in a required time of approximately 43 400 years. Even considering that OH diffusion is more rapid than that of oxygen, the available 3000 years to have attained this profile by diffusion seems somewhat insufficient, unless the system was relatively water-rich to enhance the diffusion rate at some point in its evolution. More complete understanding of the origin of water concentration gradations in crystals adjacent to melt inclusions awaits father diffusion coefficient data for water species in a variety of feldspar structural types and more mapping of well-characterized samples.

Anorthoclase/melt water concentration relationship. One of the goals of this study was to begin to explore the relationship between water concentration in feldspar and in the melt from which the feldspar crystallized. Using a broad average concentration of water in melt inclusions (~1200 ppm), compared to that in anorthoclase crystals (~130 ppm), it appears that the proportionality is approximately 10:1. However, it seems unlikely that the proportionality will remain constant in situations where anorthoclase crystallizes from melts with greater water concentrations. Rather, the crystals are likely to be saturated in water at relatively low water concentrations. Furthermore, because of the large variation in water concentrations in melt inclusions, an average melt inclusion water concentration is virtually meaningless, rendering any crystal/melt water concentration proportionality likewise meaningless, except as a way to get a general qualitative sense of the compatibility or incompatibility of water in feldspar.

The origin of differences in melt inclusion water concentrations is an intriguing question that warrants further investigation. Although this study included a preliminary test of the hypothesis that differences in melt inclusion water concentrations might represent a systematic change in water concentrations in the parent melt over the course of crystallization of anorthoclase, and that melt inclusion water concentrations might systematically vary from crystal core to rim, this hypothesis should be tested more rigorously before it is rejected. Alternatively, it is intriguing to consider the possibility that variation in water concentrations in melt inclusions might reflect real heterogeneity in water concentrations in the melt.

Summary

FTIR spectra in the range corresponding to OH^- stretches (3000–3700 cm^{-1}) for (100), (010), and (001) sections of anorthoclase from Mt. Erebus are all characterized by a broad symmetric band. Characteristics and size of the band vary little with orientation of the crystal. Following the method suggested by Libowitzky and Rossman (1997), summing the integrated area of the band from each of the three crystallographic orientations, and using the universal absorption coefficient of Johnson and Rossman (2003), the calculated water concentration of anorthoclase measured in this study is approximately 126 ppm. FTIR spectra of melt inclusions are distinguished by a broad asymmetric band centered at 3300–3500 cm^{-1}. The absence of a band at 1630 cm^{-1}, which would be produced by molecular H_2O, suggests that water occurs as OH in the melt inclusions. The average water concentration in melt inclusions measured from (100), (010), and (001) sections is approximately 1500 ppm, suggesting that the proportionality between melt water concentrations and anor-

thoclase water concentration *at these low melt water concentrations* is on the order of 10:1. However, the broad range of water concentrations in melt inclusions renders this proportion useful only as a general statement regarding the relative incompatibility of water in feldspar, which comes as no surprise. Maps of water concentrations in melt inclusions, in their anorthoclase host, and in pyroxene crystals within melt inclusions, indicate that water concentration is generally homogeneous across melt inclusions, except for its high concentration in fractures. High water concentrations in fractures may result from diffusion of water to zones of lower confining pressure. Most anhydrous minerals in contact with melt inclusions have border zones up to approximately 50 μm wide, with higher water concentrations than the interior of the mineral; these zones may preserve evidence for limited diffusion of water into the mineral.

This study confirms the existence of water, albeit at low concentrations, in anorthoclase crystals as well as in melt inclusions, in the volcanic setting. The next step in investigating the partitioning of water between melt and feldspar crystals should focus on melts that are more water-rich than the Mt. Erebus phonolite, and the feldspar crystals that grow from them. In addition, further work to test hypotheses regarding the spatial distribution of melt inclusions of contrasting bulk water concentrations may provide data about the degree of heterogeneity in melts. Finally, the ability to map concentrations of water, and various species of water, in areas of interest on samples provides a basis for both establishing and testing hypotheses concerning water distribution in igneous systems.

ACKNOWLEDGMENTS

We thank the staff of the National Synchrotron Light Source at Brookhaven National Laboratory for granting us beamtime on beamline X26A. We are grateful for help and advice from G. Rossman, E. Johnson, L. Miller, and R. Smith, and for reviews of the manuscript by G. Rossman and an anonymous reviewer. We thank M. Williams and P. Low for reviews of preliminary drafts of the manuscript, and J. Sweeney for producing sample holders for thin rock slices. This work was supported by NSF grants EAR-0229607 and EAR-0229739, and by NASA grant 5-12848.

REFERENCES CITED

Aines, R.D. and Rossman, G.R. (1984) Water in minerals? A peak in the infrared. Journal of Geophysical Research, 89, 4059–4071.

Anderson, A.T., Jr. (1983) Oscillatory zoning of plagioclase; Nomarski interference contrast microscopy of etched polished sections. American Mineralogist, 68, 125–129.

——— (1989) Volcanic outgassing inferred from melt inclusions. International Geologic Congress, Abstracts, 28, 41.

Bell, D.R. and Rossman, G.R. (1992) Water in Earth's mantle: The role of nominally anhydrous minerals. Science, 255, 1391–1397.

Bell, D.R., Ihinger, P.D., and Rossman, G.R. (1995) Quantitative analysis of trace OH in garnet and pyroxenes. American Mineralogist, 80, 465–474.

Borisova, A.Y., Nikogosian, I.K., Scoates, J.S., Weis, D., Damasceno, D., Shimizu, N., and Touret, J.L.R. (2002) Melt, fluid and crystal inclusions in olivine phenocrysts from Kerguelen plume-derived picritic basalts; evidence for interaction with the Kerguelen Plateau lithosphere. Chemical Geology, 183, 195–220.

Brady, J.B. (1995) Diffusion data for silicate minerals, glasses, and liquids, p. 269–290. In T.H. Ahrens, Ed., Handbook of Physical Constants. Ref Shelf 2, American Geophysical Union, Washington, D.C.

Brophy, J.G., Dorais, M.J., Donnelly-Nolan, J.M., and Singer, B.S. (1996) Plagioclase zonation styles in hornblende gabbro inclusions from Little Glass Mountain, Medicine Lake Volcano, California; implications for fractionation mechanisms and the formation of compositional gaps. Contributions to Mineralogy and Petrology, 126, 131–136.

Burton, M.R., Oppenheimer, C., Horrocks, L.A., and Francis, P.W. (2000) Remote sensing of CO_2 and H_2O emission rates from Masaya volcano, Nicaragua. Geology, 28, 915–918.

Chakraborty, K.R. and Lehmann, G. (1976) Distribution of OH in synthetic and natural quartz crystals. Journal of Solid State Chemistry, 17, 305–311.

Cottrell, E., Gardner, J.E., and Rutherford, M.J. (1999) Petrologic and experimental evidence for the movement and heating of the pre-eruptive Minoan rhyodacite (Santorini, Greece). Contributions to Mineralogy and Petrology, 135, 315–337.

Derdau, D., Freer, R., and Wright, K. (1998) Oxygen diffusion in anhydrous sanidine feldspar. Contributions to Mineralogy and Petrology, 133, 199–204.

Dixon, J.E. and Clague, D.A. (2001) Volatiles in basaltic glasses from Loihi seamount, Hawaii: evidence for a relatively dry plume component. Journal of Petrology, 42, 627–654.

Dixon, J.E., Stolper, E., and Delaney, J.R. (1988) Infrared spectroscopic measurements of CO_2 and H_2O glasses in the Juan de Fuca Ridge basaltic glasses. Earth and Planetary Science Letters, 90, 87–104.

Dixon, J.E., Clague, D.A., and Stolper, E.M. (1991) Degassing history of water, sulfur, and carbon in submarine lavas from Kilauea Volcano, Hawaii. Journal of Geology, 99, 371–394.

Dodd, D.M. and Fraser, D.B. (1967) Infrared studies of the variation of H-bonded OH in synthetic alpha-quartz. American Mineralogist, 52, 149–160.

Dowty, E. (1978) Absorption optics of low-symmetry crystals—application to titanian clinopyroxene spectra. Physics and Chemistry of Minerals, 3, 173–181.

Dunbar, N.W. and Hervig, R.L. (1992) Petrogenesis and volatile stratigraphy of the Bishop Tuff; evidence from melt inclusion analysis. Journal of Geophysical Research, 97, 15129–15150.

Dunbar, N.W., Cashman, K.V., and Dupré, R. (1994) Crystallization processes of anorthoclase phenocrysts in the Mount Erebus magmatic system: evidence from crystal composition, crystal size distributions, and volatile contents of melt inclusions. In P.R. Kyle, Ed., Volcanological and Environmental Studies of Mount Erebus, Antarctica. Antarctic Research Series, 66, 129–146. American Geophysical Union, Washington, D.C.

Fedele, L., Bodnar, R.J., DeVivo, B., and Tracy, R. (2003) Melt inclusion geochemistry and computer modeling of trachyte petrogenesis at Ponza, Italy. Chemical Geology, 194, 81–104.

Gardner, J.E., Rutherford, M., Carey, S., and Sigurdsson, H. (1995) Experimental constraints on pre-eruptive water contents and changing magma storage prior to explosive eruptions of Mount St. Helens volcano. Bulletin of Volcanology, 57, 1–17.

Goff, F., Janik, C.J., Delgado, H., Werner, C., Counce, D., Stimac, J.A., Siebe, C., Love, S.P., Williams, S.N., Fischer, T.P., and Johnson, L. (1998) Geochemical surveillance of magmatic volatiles at Popocatepetl Volcano, Mexico. Geological Society of America Bulletin, 110, 695–710.

Hofmeister, A.M. and Rossman, G.R. (1985) A spectroscopic study of irradiation coloring of amazonite: structurally hydrous, Pb-bearing feldspar. American Mineralogist, 70, 794–804.

Ihinger, P.D. and Zink, S.I. (2000) Determination of relative growth rates of natural quartz crystals. Nature, 404, 865–869.

Jambon, A., Zhang, Y., and Stolper, E.M. (1992) Experimental dehydration of natural obsidian and estimation of D_{H2O} at low water contents. Geochimica et Cosmochimica Acta, 56, 2931–2835.

Johnson, E.A. and Rossman, G.R. (2003) The concentration and speciation of hydrogen in feldspars using FTIR and ^{1}H MAS NMR spectroscopy. American Mineralogist, 88, 901–911.

Kats, A. (1962) Hydrogen in alpha-quartz. Phillips Research Report, 17, 133–279.

Kronenberg, A.K., Yund, R.A., and Rossman, G.R. (1996) Stationary and mobile hydrogen defects in potassium feldspar. Geochimica et Cosmochimica Acta, 60, 4075–4094.

Libowitzsky, E. and Rossman, G.R. (1997) An IR absorption calibration for water in minerals. American Mineralogist, 82, 1111–1115.

Mackwell, S.J. and Paterson, M.S. (1985) Water-related diffusion and deformation effects in quartz at pressures of 1500 and 300 Mpa, p. 141–150. In R.N. Schock, Ed., Point Defects in Minerals. Geophysical Monograph Series, AGU, Washington, D.C.

Mandeville, C.W., Webster, J.D., Rutherford, M.J., Taylor, B.E., Timbal, A., and Faure, K. (2002) Determination of molar absorptivities for infrared absorption bands of H_2O in andesitic glasses. American Mineralogist, 87, 813–821.

McMillan, P.F., Akaogi, M., Sato, R.K., Poe, B., and Foley, J. (1991) Hydroxyl groups in β-Mg_2SiO_4. American Mineralogist, 76, 354–360.

Nakashima, S., Matayoshi, H., Yuko, T., Michibayashi, K., Masuda, T., Kuroki, N., Yamagishi, H., Ito, Y., and Nakamura, A. (1995) Infrared microspectroscopy analysis of water distribution in deformed and metamorphosed rocks. Tectonophysics, 245, 263–276.

Naney, M.R. (1983) Phase equilibria of rock-forming ferromagnesian silicate in granitic systems. American Journal of Science, 283, 993–1033.

Newman, S., Stolper, E.M., and Epstein, S. (1986) Measurement of water in rhyolitic glasses: calibration of an infrared spectroscopic technique. American Mineralogist, 71, 1527–1541.

Ohlhorst, S., Behrens, H., and Holtz, F. (2001) Compositional dependence of molar absorptivities of near-infrared OH^- and H_2O bands in rhyolitic to basaltic glasses. Chemical Geology, 174, 5–20.

Scaillet, B., Pichavant, M., and Roux, J. (1995) Experimental crystallization of leucogranite magmas. Journal of Petrology, 36, 663–705.

Singer, B.S. and Pearce, T.H. (1993) Plagiocalse zonation in a basalt to rhyodacite

eruptive suite, Seguam Island, Alaska; observations by Nomarski contrast interference. Canadian Mineralogist, 31, 459–466.
Smyth, J.R. (1987) β-Mg_2SiO_4: A potential host for water in the mantle? American Mineralogist, 72, 1051–1055.
Smyth, J.R., Bell, D.R., and Rossman, G.R. (1991) Incorporation of hydroxyl in upper mantle clinopyroxenes. Nature, 351, 732–735.
Stolper, E. (1982) Water in silicate glasses: An infrared spectroscopic study. Contributions to Mineralogy and Petrology, 81, 1–17.
Walker, J.A., Roggensack, K., Patino, L., Cameron, B.I., and Matias, O. (2003) The water and trace element contents of melt inclusions across an active subduction zone. Contributions to Mineralogy and Petrology, 146, 62–77.
Whitney, J.A. (1988) The origin of granite; the role and source of water in the evolution of granitic magmas. Geological Society of America Bulletin, 100, 1886–1897.
Wiebe, R.A. (1968) Plagioclase stratigraphy: a record of magmatic conditions and events in a granite stock. American Journal of Science, 266, 690–703.
Wilkins, R.W.T. and Sabine, W. (1973) Water content of some nominally anhydrous silicates. American Mineralogist, 58, 508–516.
Zhang, Y. and Behrens, H. (2000) H_2O diffusion in rhyolitic melts and glasses. Chemical Geology, 169, 243–262.
Zhang, Y. and Stolper, E.M. (1991) Water diffusion in a basaltic melt. Nature, 351, 306–309.
Zhang, Y., Stolper, E.M., and Wasserburg, G.J. (1991) Diffusion in rhyolitic glasses. Geochimica et Cosmochimica Acta, 55, 441–456.
Zhang, Y., Stolper, E.M., and Ihinger, P.D. (1997) Kinetics of the reaction H_2O + O = 2 OH in felsic glasses: preliminary results. American Mineralogist, 80, 593–612.

MANUSCRIPT RECEIVED JULY 12, 2004
MANUSCRIPT ACCEPTED APRIL 20, 2005
MANUSCRIPT HANDLED BY LEE A. GROAT